Article

Enhanced Mechanical Toughness of Isotactic Polypropylene Using Bulk Molybdenum Disulfide

Vijay S Wadi, Kishore K. Jena, Kevin Halique, and Saeed M. Alhassan*

Cite This: *ACS Omega* 2020, 5, 11394−11401

Read Online

ACCESS | Metrics & More | Article Recommendations | Supporting Information

ABSTRACT: Herein, we report the use of bulk molybdenum disulfide (MoS_2) as the reinforcing agent to enhance the toughness of isotactic polypropylene (iPP). The iPP-MoS_2 nanocomposites with varying amounts of MoS_2 (0.1 to 5 wt %) were prepared by a one-step melt extrusion method, and the effects of MoS_2 on the morphology, thermal, and mechanical properties were evaluated by different instrumental techniques such as Raman, ATR-FTIR, UTM, TEM, TGA, and DSC. TEM images showed the uniform dispersion of multilayer MoS_2 in the polymer matrix, and XRD results suggested the formation of the β phase when a low amount of MoS_2 is loaded in the composites. Mechanical tests revealed a significant increase in the toughness and elongation at break (300−400%) in the composites containing low amounts of MoS_2 (0.25 to 0.5 wt %). Enhanced toughness and elongation in iPP could be related to the combined effect of the β phase and the exfoliation of bulk MoS_2 under applied stress. The thermal stability of the composites was also improved with the increase in MoS_2 loading. Direct utilization of bulk MoS_2 and one-step melt extrusion process could be a cost-effective method to induce high elasticity and toughness in iPP.
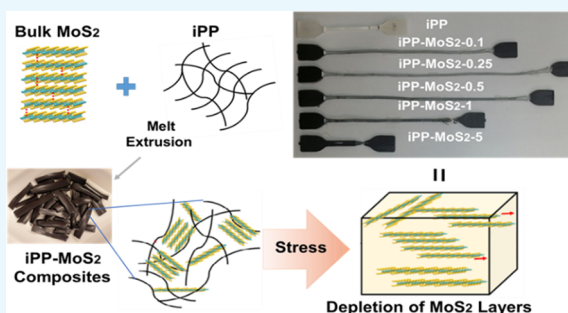
INTRODUCTION

Polypropylene (PP) is the second-most widely produced commodity plastic. It is used in a variety of applications because of its low cost, excellent mechanical properties, easy process, and recyclability.[1−3] Due to its superior property and easy availability, PP has attracted many researchers and has been studied extensively in its pristine state as well as in composites using various fillers such as silica particles, clay, talc, calcium carbonate, mica, graphite particles, graphene, carbon black, and carbon nanotubes (CNTs) to meet the desired applications.[4−10]

The properties of PP are mainly governed by crystallinity induced by the orientation of methyl groups; thus, PP exists in different crystalline forms. Isotactic polypropylene (iPP) possesses the highest degree of crystallinity and shows superior properties due to the highly ordered arrangements of methyl groups. Due to this, iPP also exhibits a relatively high brittle point compared to the engineered plastics, which could limit its applications.

Addition of a plasticizer is one way to decrease the brittleness and improve the elasticity of the polymer. Plasticizers such as mineral oil, paraffin, or esters are commonly used to alter the polymer properties. However, use of the plasticizer can also lead to lower tensile strength and/or adversely affect other physical properties. The liquid plasticizers volatilize and oxidize under moderate to high temperatures, which can decrease the performance of the polymer over time. The plasticizers also have a major drawback of leaching out from the polymer on long-term use.[11−13]

The properties of the iPP can also be altered by controlling the crystalline phases and morphologies like monoclinic α phase, β phase, or γ phase under crystallization conditions. These crystalline phases induce different properties to the polymer.[14,15] Among these phases, the β-crystalline phase reduces the brittleness and improves the toughness of the polymer and also exhibits a low modulus of elasticity, higher ductility, and impact strength compared to the α phase.[15−19] Thus, many researchers studied the β-nucleating efficiency and its effect on the crystallization behavior, melting characteristics, and mechanical properties.[20−24]

Molybdenum disulfide (MoS_2) structures contain molybdenum atoms sandwiched between two layers of sulfur atoms. The bulk MoS_2 is a multilayered structure of these 2D layers stacked together by weak van der Waals forces, and these layers can easily separate and slide under the friction shearing. Hence, MoS_2 has a low friction coefficient and becomes an important solid lubricant in oils, coating, aviation, and aerospace.[25−27]
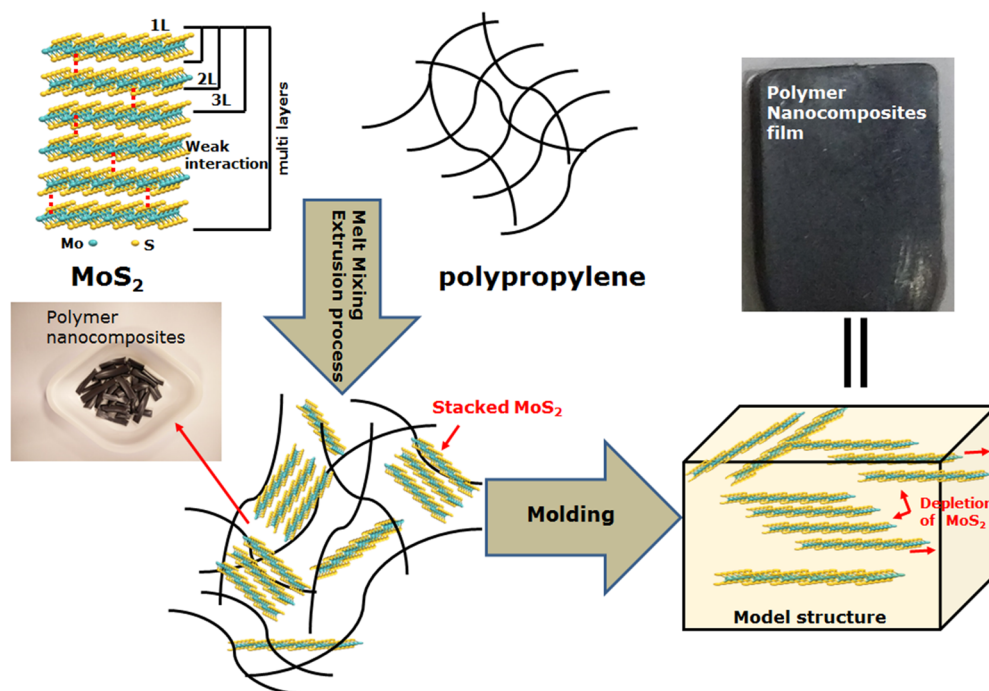
11394

Scheme 1. Overall Polymer Nanocomposite Preparation Method and the iPP-MoS₂ Nanocomposite Film Preparation for Mechanical and Electron Microscope Studies


Because of its exciting properties, MoS₂ is also combined with polymers to change crystallization behavior, to increase toughness, and to improve thermal stability and tribological properties.[28]

In this work, the bulk MoS₂ powder is directly used as the filler to prepare iPP-MoS₂ composites, and the effect of MoS₂ loading on the crystallization, thermal, and mechanical behavior is studied. The composites were successfully fabricated through a one-step melt extrusion method. A possible crystallization growth and crystallinity of the composites are presented in detail based on DSC and XRD studies. Furthermore, the mechanical performances of the iPP composites are investigated and discussed with respect to MoS₂ loading.

RESULTS AND DISCUSSION

A general schematic illustration for the preparation of iPP-MoS₂ composites is shown in Scheme 1. Various amounts of multilayer bulk MoS₂ were directly loaded into the iPP matrix, and the effect on the thermal and mechanical properties was studied.

The Raman and ATR-FTIR spectra of iPP-MoS₂ nanocomposites along with bulk MoS₂ and pure iPP are presented in Figure 1. The stacked structure of bulk MoS₂ was confirmed through the measurement of E^1_{2g} and A_{1g} peak positions in the Raman spectra. The appearance of two characteristic peaks at 391 and 411 cm^{-1} corresponded to the E^1_{2g} and A_{1g} vibrational modes of hexagonal MoS₂, respectively.[29] The E^1_{2g} mode related to the in-plane vibration, i.e., sulfur atoms in the opposite direction to the Mo atom, while the A_{1g} mode represents the out-of-plane vibration where the sulfur atoms are in the opposite direction.[30] In Figure 1a, E^1_{2g} and A_{1g} peaks of MoS₂ in the nanocomposites shift by 20 cm^{-1} to the higher frequency and merged with the iPP peaks, which indicate the presence of few layers or exfoliated layers of MoS₂.[31] The
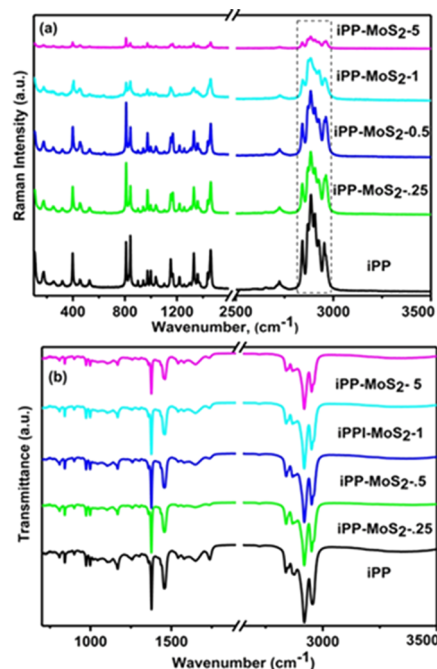
Figure 1. (a) Raman spectra of iPP and iPP-MoS₂ hybrid composites and (b) Raman spectra of bulk hexagonal MoS₂.

characteristic bands at 2963, 2902, 2879, and 2842 cm^{-1} in the iPP-MoS₂ nanocomposites are mainly attributed to the symmetric and asymmetric vibration of CH₂ and CH₃ groups, corresponding to the alkyl chains of iPP. Furthermore, the C—S stretching in 710−570 cm^{-1} absorption does not appear in the composites indicating the lack of chemical bonding between iPP and MoS₂. ATR-FTIR measurements of the composites are presented in Figure 1b, showing the major peaks related to both iPP and bulk MoS₂ (see Figure S2), and
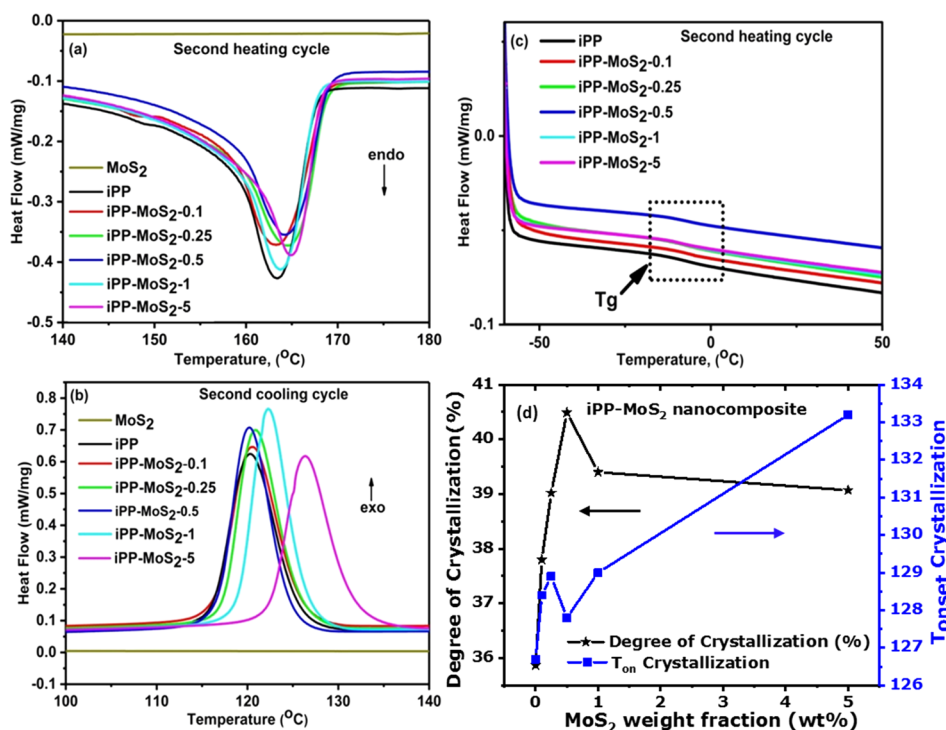
Figure 2. Enlarged portion of DSC curves. (a) Second heating; (b) second cooling cycle of MoS_2, iPP, and iPP-MoS_2 hybrid composites; (c) comparing T_g curves of iPP and iPP-MoS2 hybrid composites; (d) correlation between the crystalline degree (%) and crystallization onset temperature and MoS_2 weight fraction (%).

Table 1. Melting Temperatures (T_m), Fusion Enthalpies (ΔH_m), Crystallization Temperatures (T_c), and Degrees of Crystallinity (X_c) of iPP-MoS_2 Nanocomposites

nanocomposite	T_g (°C)	T_m (°C)	ΔH_m (cal/g)	T_c (°C)	ΔH_c (cal/g)	X_c^a (%)
iPP	−9.73	163.11	74.27	120.20	72.12	35.87
iPP-MoS_2-0.1	−9.11	163.43	78.24	120.60	76.77	37.8
iPP-MoS_2-0.25	−8.78	164.58	80.79	120.93	80.34	39.02
iPP-MoS_2-0.5	−9.81	164.44	83.82	120.12	80.96	40.49
iPP-MoS_2-1	−9.16	163.69	81.71	122.23	79.51	39.4
iPP-MoS_2-5	−9.35	164.79	80.89	126.24	82.14	39.07

^{a}Determined using the following equation: X_c (%) = $\Delta H_m / \Delta H_m^\circ \times 100$, where ΔH_m° = 207 J/g is the theoretical enthalpy value for a 100% crystalline iPP.

as expected, no new peaks appeared in the composites suggesting the physical mixing of iPP and MoS_2.

Complete thermograms from −50 to 200 °C for the iPP-MoS_2 composites are presented in Figure S3. Enlarged DSC thermograms of second heating and cooling cycles of iPP, MoS_2, and their composites are presented in Figure 2a,b, respectively. The area under the curve and peak position in DSC indicate the degree of crystallization of the polymer. It can be clearly observed that the peak position and areas of the melting and crystallization peaks increase with increasing MoS_2 loading and shift to the right compared to those of the pure iPP. The increased areas of melting (enthalpy (ΔH_m)) and crystallization peaks (enthalpy (ΔH_c)) in the nanocomposites suggest the role of MoS_2 as a nucleating agent in the matrix.

The degree of crystallinity is an important parameter to study the crystallization properties of the nanocomposites. The degree of crystallinity (X_c, %) is calculated using the below equation

$$\text{degree of dcrystallinity } X_c(\%) = (\Delta H_m / \Delta H_m^\circ) \times 100 \quad (1)$$

where ΔH_m is the thermal enthalpy of the composite and ΔH_m° is the thermal enthalpy for 100% crystalline polymer. The enthalpy of 100% crystalline isotactic polypropylene (iPP) (ΔH_m°) is 207 J/g and is used as reference.[32]

The degrees of crystallinity in the iPP-MoS_2 nanocomposites determined from the experimental measurements using eq 1 are given in Table 1. The crystallization behavior of the polymer can be characterized by the onset temperature of the crystalline peak. Figure 2d presents the relationship between the onset crystallization temperature (T_{onset}) and the MoS_2 weight fraction. The onset crystallization temperatures in the iPP composites increase with increasing MoS_2 loading from 127 to 133 °C. The composites showed a higher degree of crystallinity (%) when the weight fraction of MoS_2 loading is lower than 0.5 wt %; however, the degree of crystallinity (%) varies irregularly with further increasing MoS_2 loading. Moreover, the degree of crystallinity of the nanocomposites is obviously higher than that of the unfilled iPP at all MoS_2 weight fractions. This suggests the heterogeneous nucleation role of MoS_2 in the iPP matrix, resulting in the increase in the

degree of crystallinity of the nanocomposites, specifically in the case of lower MoS_2 (0.1–0.5) loading.

Generally, the crystallization behavior of polymer-inorganic composites depends on the processing condition of the polymer (i.e., cooling rate) and the heterogeneous nucleation effect induced by the inorganic filler materials. The heterogeneous nucleation effect is closely related to the interaction between the fillers and the polymer matrix. Inorganic fillers at low concentration are relatively easy to disperse in the polymer matrix, and hence, at low concentration, the interaction between the filler and polymer is considerably high; this leads to an increase in the heterogeneous nucleation effect and increases the crystalline degree in the composites. However, when the concentration of the filler increased above a certain percentage, the uniform dispersion of fillers in the polymer matrix becomes difficult, and particles start to aggregate; thus, the interaction between the filler and the polymer matrix weakens and leads to the instability in the degree of crystallinity.

Interaction between the MoS_2 and iPP matrix is also closely related to the size, specific surface area, and morphology of the MoS_2. The specific surface area of the MoS_2 at lower concentration improves the interaction with the polymer matrix and increases the crystallinity. It can be seen in Table 1 that the degrees of crystallinity of the iPP-MoS_2 composites increased with an increase in the MoS_2 amount from 0.1 to 0.5 wt %; however, a further increase in the loading resulted in reduced crystallinity due to the agglomeration of MoS_2 layers. The formation of β crystals was also observed when a lower amount of MoS_2 was used (see Figure S4), indicating the ability of MoS_2 to form β crystals. The amount of β crystals was much lower than that of the α form and was completely absent when more than 0.5 wt % MoS_2 was used, which could be due to the decrease in the heterogeneous nucleation at higher MoS_2 loading. This result supports the increase in the iPP crystallinity at a low amount of MoS_2. Thus, a small amount of MoS_2 is beneficial to control the total crystallization rate of the iPP-MoS_2 composites. The glass transition temperatures of iPP-MoS_2 nanocomposites are presented and reported in Table 1 and Figure 2c. Glass transition temperature did not show a significant change with MoS_2 addition.

The effect of MoS_2 on the crystallization behavior of the iPP was investigated by XRD. Figure S5 shows the comparison of pure MoS_2 and iPP with the iPP-MoS_2 composites. The highly crystalline multilayered structure of MoS_2 displays a diffraction peak at 2θ = 14.4, 32.6, and 39.7, corresponding to the (002), (100), and (103) planes.[33] Similarly, iPP shows partially crystalline diffraction peaks at 2θ = 14.2, 17, and 19.1°, attributed to the α (110), α (040), and α (130) planes,[34] respectively. However, a new peak at 16° appeared in iPP-MoS_2 composites with low MoS_2 loading, assigned to the β (300) phase. The shift in the iPP peak position from 14.2 to 14.4° indicates the formation of the β phase.[34,35] Moreover, under the same processing conditions, iPP does not show the presence of the β phase and confirms the effective role of MoS_2 as the β-nucleating agent. This result is also in good agreement with the shift in the melt transition of iPP-MoS_2 composites with the addition of MoS_2 in DSC. The other peaks of iPP-MoS_2 composites are similar to those of iPP except the overlapping of the (002) MoS_2 peak with the iPP (110) plane (Figure 3). Further, no noticeable diffraction peaks associated with the (100), (103), and (105) planes of MoS_2 appear in the composites, implying the possible decrease in the stacking of
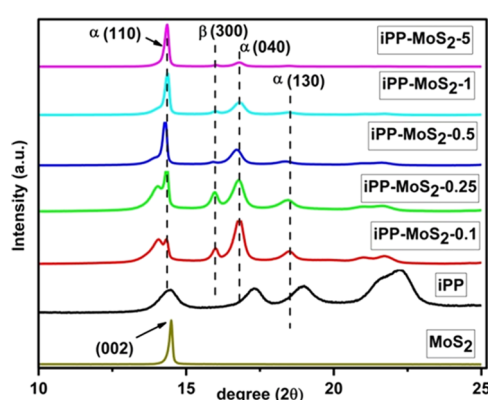

Figure 3. XRD patterns of pure iPP and iPP-MoS_2 composites (expanded zone: scale 10−25°).

MoS_2 layers in the composites. This could be due to the partial exfoliation of the MoS_2 layers during melt extrusion, which reduces the number of multilayer crystalline structures. Further, the XRD of the stretched part of iPP-MoS_2 composites after the UTM test is also presented in Figure S6 and shows destruction in the crystalline arrangement under applied stress. The major crystalline peaks of iPP disappeared after the stress−strain test, implying that the crystalline lamellar in the samples absorbed the applied stress and led to the elastic nature. Similarly, the intensities of the sharp crystalline peaks of MoS_2 in the composites that also significantly reduced with respect to iPP crystalline peaks suggest the decrease in lamellar thickness of MoS_2. A decrease in lamellar thickness also suggests the exfoliation of MoS_2 layers under stress. However, in the samples with higher amounts of MoS_2, the crystalline peaks that still appeared with high intensity indicate the aggregation and intact MoS_2 layers.

Mechanical properties of the composites mainly depend on the amount and dispersion of the fillers inside the polymer matrix. The effects of MoS_2 on the mechanical properties like tensile strength, elongation at break, and toughness of the pristine iPP and the iPP-MoS_2 nanocomposites are presented in Figure 4, and the results are listed in Table S1. Young's modulus calculated from the slope is given in Figure S7. Figure 4a shows the stress−strain curves of pure iPP and iPP-MoS_2 composites with various amounts of MoS_2 loading. The results show that the iPP-MoS_2 composites exhibit a significantly better performance than the pristine iPP. The composites with 0.25 and 0.5 wt % MoS_2 loadings showed the highest elongation at break, without much decrease in tensile strength, clearly indicating the dramatic enhancement of toughness in the composites. The stress−strain profiles (Figure 4a) also revealed an up to 700−800% improvement in the elasticity of the iPP with low amounts of MoS_2 (0.25−0.5 wt %) loading and the minimum elongation (41%) for 5 wt % MoS_2. The digital images of the corresponding samples after the mechanical test are presented in Figure 4b and clearly suggest enhanced elastic properties of the samples with low amounts of MoS_2. This can be related to the depletion of multilayer MoS_2 under applied stress during the test. When stress is applied to the composites, the bulk MoS_2 absorbs the stress and leads to the depletion of the multilayer structure due to the weak intermolecular interaction (van der Waals force of attraction) between MoS_2 layers.[26,27,36−39] Thus, the bulk MoS_2 exfoliates in the polymer matrix and decreases the resistance to fracture when receiving external force and behaves as a solid lubricant.
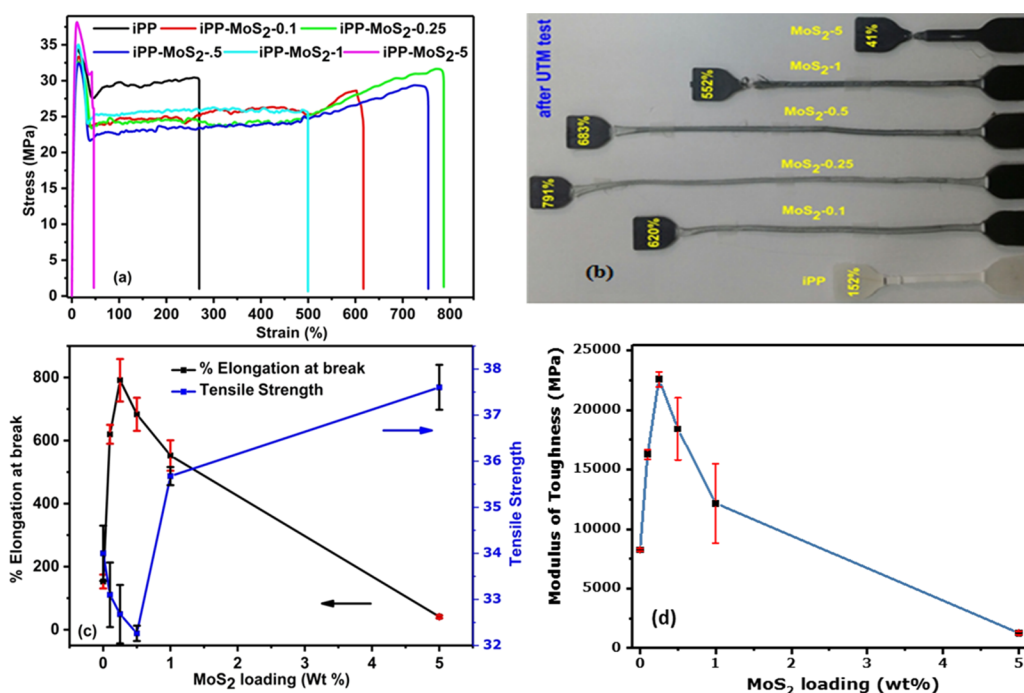
Figure 4. Mechanical properties of iPP-MoS$_2$ composites: (a) stress and strain (%) curves of iPP and iPP-MoS$_2$ composites; (b) digital image of iPP-MoS$_2$ composites after mechanical testing; (c) comparison of elongation at break and tensile strength at different MoS$_2$ loading percentages; (d) toughness of iPP-MoS$_2$ composites with respect to MoS$_2$ loading calculated by the area under the stress−strain curves.
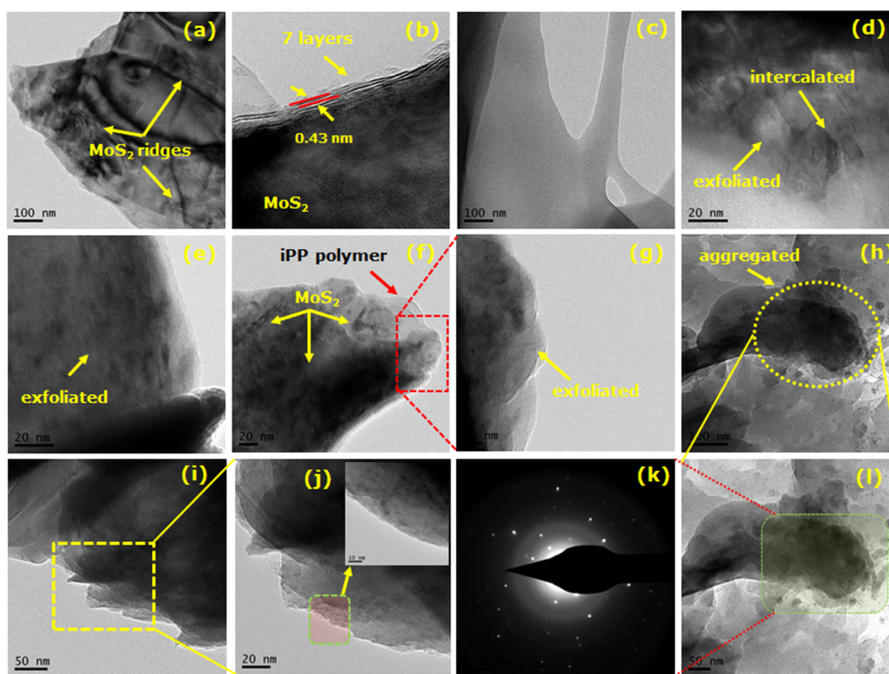
Figure 5. TEM images of bulk MoS$_2$, iPP, and iPP-MoS$_2$ hybrid composites. (a,b) Bulk MoS$_2$: MoS$_2$ ridges and layer structure; (c) pure iPP; (d) iPP-MoS$_2$-0.1 (exfoliated and intercalated structure); (e) iPP-MoS$_2$-0.25 (exfoliated structure); (f) iPP-MoS$_2$-0.5; (g) iPP-MoS$_2$-0.5 (expanded zone); (h) iPP-MoS$_2$-1; (i) iPP-MoS$_2$-5; (j) iPP-MoS$_2$-5 (expanded zone: high resolution of the expanded zone (inset), 10 nm); (k) iPP-MoS$_2$-1 (single area diffraction pattern); (l) iPP-MoS$_2$-1 (expanded zone: aggregated morphology).

Moreover, the presence of the β phase confirmed from XRD also contributes to improving ductility of the iPP. Thus, the combined effect of exfoliation or depletion of MoS$_2$ layers and the presence of the β phase can be attributed to the enhanced elasticity of the composites.

The ultimate tensile strength (UTS) of the composites slightly decreased for low-MoS$_2$-loaded samples, i.e., 33.1, 32.68, and 32.26 MPa, for 0.1, 0.25, and 0.5 wt % MoS$_2$, respectively. However, increasing MoS$_2$ to 1 and 5 wt % resulted in increased strength to 35.6 and 37.6 MPa, respectively. Young's modulus calculated by measuring the slope at the linear region of the stress−strain curves (see Figure S7) also shows a similar trend that the modulus decreased in low MoS$_2$ loading and increased at high amounts

of MoS$_2$. The details of the mechanical properties measured for the composite samples are listed in Table S1.

Toughness is the area under the stress vs strain curve determined by tensile testing[40−42] and is shown in Figure 4d. The iPP-MoS$_2$ composites with 0.25 and 0.5 wt % MoS$_2$ showed higher resistance to break and showed high flexibility without a significant decrease in the tensile strength. However, this behavior was not observed in high-MoS$_2$-loaded samples, which could be due to the aggregation of MoS$_2$ sheets and the absence of the β phase. Aggregation of MoS$_2$ layers can potentially reduce the exfoliation of layers and enhance the modulus (see Figure S7).

The partial exfoliated structure of MoS$_2$ in iPP composites was further supported by the TEM images in Figure 5. The ultrathin sections obtained from microtome of iPP, iPP-MoS$_2$-0.1, iPP-MoS$_2$-0.25, iPP-MoS$_2$-0.5, iPP-MoS$_2$-1, and iPP-MoS$_2$-5 are depicted in Figure 5. The TEM image of bulk MoS$_2$ in Figure 5a,b shows the layer structure and ridges in the bulk MoS$_2$, and the distance between layers was approximately 0.5 nm. However, in Figure 5d−f, for iPP-MoS$_2$ composites, the lamellar morphology of MoS$_2$ nanosheets can be seen at lower concentration and is well dispersed. TEM images also show the bilayer or trilayer MoS$_2$ nanosheets in the hybrid composites.[36,43] This could be due to the partial exfoliation of MoS$_2$ layers under melt extrusion sheering and mixing conditions. It is clearly observed that most of the MoS$_2$ with thin morphology are uniformly dispersed in the iPP matrix without significant aggregation when a low amount of MoS$_2$ was used; however, increasing the amount of MoS$_2$ resulted in the agglomeration of the multilayer structure (see Figure 5f,j). All composites exhibited homogeneity, and no sign of phase separation was found. The combination of the selected area electron diffraction (SAED) pattern (Figure 5k) confirms the presence of the MoS$_2$ crystal lattice in the composites.

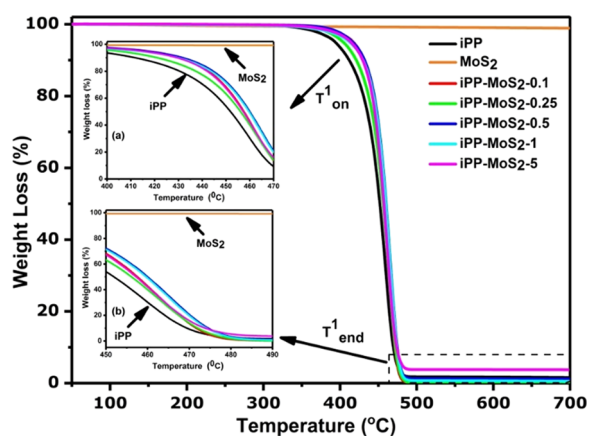Figure 6 shows the TGA curves of iPP and iPP-MoS$_2$ composites, and the corresponding values are presented in

Figure 6. TGA profiles of iPP and iPP-MoS$_2$ nanocomposites.

Table 2. The thermogram and DTG curves (see Figure S8) of iPP and iPP-MoS$_2$ composites show single-stage decomposition, and the bulk MoS$_2$ is thermally stable up to 700 °C. Pure iPP initial degradation starts at around 394 °C, shows maximum degradation at 415 °C, and completely degrades at 485 °C. Meanwhile, thermal stability of the iPP-MoS$_2$ nanocomposites increases with increasing MoS$_2$ loading. Addition of a small amount of MoS$_2$ (0.1 wt %) significantly improves the initial degradation also indicating the uniform

Table 2. Thermal Data of iPP-MoS$_2$ Nanocomposites

nanocomposite	T^1_{on} (°C)	T^1_{end} (°C)	T^1_{max} (°C)	residue (500 °C)
iPP	394.0	479.4	451.1	0.77
iPP-MoS$_2$-0.1	417.5	481.8	452.3	1.1
iPP-MoS$_2$-0.25	413.1	486.4	453.3	1.43
iPP-MoS$_2$-0.5	422.7	487.2	455.1	1.73
iPP-MoS$_2$-1	423.1	488.9	457.6	2.30
iPP-MoS$_2$-5	422.9	490.1	459.0	4.11

dispersion of MoS$_2$ in the matrix. Thermally stable MoS$_2$ layers absorb the heat in the composites and increase the degradation temperature of iPP. The residues of iPP composites at 500 °C given in Table 2 are comparable with the initial feed ratio of MoS$_2$ suggesting the complete incorporation of MoS$_2$ during the extrusion process.

CONCLUSIONS

Bulk MoS$_2$ was used as a nanofiller to prepare iPP-MoS$_2$ nanocomposites by a one-step melt extrusion process. The bulk MoS$_2$ at low amounts of loading (0.25 to 0.5 wt %) in the iPP-MoS$_2$ composites showed significant improvement in the toughness and elongation at break (300 to 400%) of the polymer. XRD confirmed the formation of the β-crystalline structure in the composites, and DSC revealed the nucleating properties of MoS$_2$ at lower concentration. An increase in the toughness and elongation at break could be due to the formation of the β-crystalline structure and also due to the sliding or exfoliation of MoS$_2$ layers under applied stress during the UTM test. TEM showed uniform dispersion of MoS$_2$ in the iPP matrix. Addition of a small amount of MoS$_2$ also improved the thermal stability of the polymer. The use of bulk MoS$_2$ and one-step melt extrusion process could be a low-cost, scalable, simple method to achieve enhanced toughness and elongation in iPP.

MATERIAL AND METHODS

Materials. Bulk molybdenum disulfide (MoS$_2$) was supplied by Composites Innovation Centre (CIC), Canada, and used without any modification. Isotactic polypropylene (iPP) with average M_n ~97000 was obtained from Aldrich, USA. The polypropylene pellets were dried at 80 °C for 24 h in an air-circulated oven before extrusion.

Sample Preparation. The iPP-MoS$_2$ composites were prepared by direct melt extrusion of MoS$_2$ and iPP using a twin-screw Haake Minilab II extruder. Initially, iPP was melted above its melting point (190 °C) in the extruder, and to this, preweighed MoS$_2$ was added gradually and allowed to mix for 30 min at 100 rpm speed. Later, the mixture was extruded through a rectangular-shaped die and allowed to cool naturally to room temperature. A similar procedure was also applied to prepared composites with varying MoS$_2$ loadings (0.1 to 5 wt %). The extrudate was cut into small pieces and used to form dumbbell shapes through the injection molding process. Injection molding was carried out by using a Thermo Scientific Haake minijet pro injection molder. The injection molding parameters are as follows: melt temperature 190 °C, mold temperature 115 °C, injection pressure 500 bar, and cooling time in excess of 60 s. All of the molded samples have a similar thickness of approximately 2 mm. The schematic diagram for the preparation of composites is shown in Scheme 1. The sample geometry used for the tensile testing is presented in

Figure S1. The samples were denoted as iPP-MoS$_2$-X, where X represents the corresponding weight percentage of MoS$_2$.

Characterization Methods. Infrared spectra of iPP and iPP-MoS$_2$ nanocomposites were recorded by attenuated total reflectance Fourier transform infrared spectroscopy (ATR-FTIR) using a Bruker Vertex 70. Differential scanning calorimetry (DSC) analysis of the nanocomposite samples (5−10 mg) was carried out using a TA Discovery DSC at a heating rate of 10 °C/min in the temperature range between −50 and 200 °C under a nitrogen environment. Thermogravimetric analysis was done with a Discovery TGA by TA Instruments. Samples (5−10 mg) were heated from 25 to 700 °C under 30 mL/min N$_2$ flow at a heating rate of 10 °C/min. The strength and plasticization effect of MoS$_2$ reinforced isotactic polypropylene (iPP) composites were studied using an Instron 2519-107, USA, universal testing machine. Tests were carried out according to ASTM standards D638 using a 100 N load cell and 10 mm/min cross head speed. The specimens were thin rectangular strips (4× 27 × 2 mm of width, length, and thickness, respectively). Tensile strength, modulus, and elongation at break values correspond to the average of five samples. Diffraction (XRD) patterns were collected using an analytical X'Pert PRO powder diffractometer (Cu Kα radiation 1.5406 Å, 40 kV, 40 mA) in the range of 5−80° 2θ scale, with a step size of 0.02°. Transmission electron microscopy (TEM) images were obtained using an FEI Tecnai G20 operated at 200 kV accelerating voltage to observe the nanoscale structures in the composites. Samples were ultra-microtomed in room-temperature conditions to prepare less than 100 nm-thick samples.

ASSOCIATED CONTENT

Ⓢ Supporting Information

The Supporting Information is available free of charge at https://pubs.acs.org/doi/10.1021/acsomega.0c00419.

Digital images of iPP and iPP-MoS$_2$ nanocomposites before UTM study. ATR-FTIR measurement the bulk MoS$_2$ powder. Second heating and cooling cycle DSC curves of iPP and iPP-MoS$_2$ hybrid composites in the range of 30 to 200 °C. XRD patterns of bulk MoS$_2$, pure iPP, and iPP-MoS$_2$ nanocomposites from 2θ = 5 to 80°. XRD of the stretched portion of iPP-MoS$_2$ nanocomposites after the UTM test. Young's moduli of composites at different loading percentages of MoS$_2$. DTG curves of bulk MoS$_2$ and nanocomposites. Table of mechanical properties of iPP and iPP-MoS$_2$ nanocomposites (PDF)

AUTHOR INFORMATION

Corresponding Author

Saeed M. Alhassan − *Department of Chemical Engineering, Khalifa University of Science and Technology, Abu Dhabi 00000, United Arab Emirates;* ⓸ orcid.org/0000-0002-5148-3255; Email: saeed.alkhazraji@ku.ac.ae

Authors

Vijay S Wadi − *Department of Chemical Engineering, Khalifa University of Science and Technology, Abu Dhabi 00000, United Arab Emirates;* ⓸ orcid.org/0000-0002-9904-3865

Kishore K. Jena − *Department of Chemical Engineering, Khalifa University of Science and Technology, Abu Dhabi 00000, United Arab Emirates*

Kevin Halique − *Department of Chemical Engineering, Khalifa University of Science and Technology, Abu Dhabi 00000, United Arab Emirates*

Complete contact information is available at:
https://pubs.acs.org/10.1021/acsomega.0c00419

Notes

The authors declare no competing financial interest.

ACKNOWLEDGMENTS

REFERENCES

(1) Suppakul, P.; Miltz, J.; Sonneveld, K.; Bigger, S. W. Active Packaging Technologies with an Emphasis on Antimicrobial Packaging and its Applications. *J. Food Sci.* **2003**, *68*, 408−420.

(2) Rhim, J.-W. Potential use of biopolymer-based nanocomposite films in food packaging applications. *Food Sci. Biotechnol.* **2007**, *16*, 691.

(3) Prasannan, A.; Jhu, J.-J.; Wu, C.-J.; Lin, S.-Y.; Tsai, H.-C. Evaluation of the temperature and molecular weight dependent migration of di(2-ethylhexyl) phthalate from isotactic polypropylene composites. *React. Polym.* **2017**, *113*, 70−76.

(4) Sun, X.; Li, H.; Wang, J.; Yan, S. Shear-Induced Interfacial Structure of Isotactic Polypropylene (iPP) in iPP/Fiber Composites. *Macromolecules* **2006**, *39*, 8720−8726.

(5) Nagendra, B.; Rosely, C. V. S.; Leuteritz, A.; Reuter, U.; Gowd, E. B. Polypropylene/Layered Double Hydroxide Nanocomposites: Influence of LDH Intralayer Metal Constituents on the Properties of Polypropylene. *ACS Omega* **2017**, *2*, 20−31.

(6) Abdou, J. P.; Reynolds, K. J.; Pfau, M. R.; van Staden, J.; Braggin, G. A.; Tajaddod, N.; Minus, M.; Reguero, V.; Vilatela, J. J.; Zhang, S. Interfacial crystallization of isotactic polypropylene surrounding macroscopic carbon nanotube and graphene fibers. *Polymer* **2016**, *91*, 136−145.

(7) Yang, K.; Yang, Q.; Li, G.; Sun, Y.; Feng, D. Mechanical properties and morphologies of polypropylene with different sizes of calcium carbonate particles. *Polym. Compos.* **2006**, *27*, 443−450.

(8) Tarapow, J. A.; Bernal, C. R.; Alvarez, V. A. Mechanical properties of polypropylene/clay nanocomposites: Effect of clay content, polymer/clay compatibility, and processing conditions. *J. Appl. Polym. Sci.* **2008**, *111*, 768−778.

(9) Gan, L.; Qiu, F.; Hao, Y.-B.; Zhang, K.; Zhou, Z.-Y.; Zeng, J.-B.; Wang, M. Shear-induced orientation of functional graphene oxide sheets in isotactic polypropylene. *J. Mater. Sci.* **2016**, *51*, 5185−5195.

(10) Qiu, F.; Hao, Y.; Li, X.; Wang, B.; Wang, M. Functionalized graphene sheets filled isotactic polypropylene nanocomposites. *Composites, Part B* **2015**, *71*, 175−183.

(11) Faessler, D.; McCombie, G.; Biedermann, M.; Felder, F.; Subotic, U. Leaching of plasticizers from polyvinylchloride perfusion lines by different lipid emulsions for premature infants under clinical conditions. *Int. J. Pharm.* **2017**, *520*, 119−125.

(12) Sander, M. M.; Nicolau, A.; Guzatto, R.; Samios, D. Plasticiser effect of oleic acid polyester on polyethylene and polypropylene. *Polym. Test.* **2012**, *31*, 1077−1082.

(13) Nitta, K.-h.; Ando, H.; Asami, T. Plasticizing of isotactic polypropylene upon addition of hydrocarbon oils. *e-Polym.*, **2004**, *4*, DOI: 10.1515/epoly.2004.4.1.212.

(14) Lotz, B.; Graff, S.; Straupé, C.; Wittmann, J. C. Single crystals of γ phase isotactic polypropylene: combined diffraction and morphological support for a structure with non-parallel chains. *Polymer* **1991**, *32*, 2902−2910.

(15) Tjong, S. C.; Shen, J. S.; Li, R. K. Y. Mechanical behavior of injection molded β-crystalline phase polypropylene. *Polym. Eng. Sci.* **1996**, *36*, 100−105.

(16) Byelov, D.; Panine, P.; Remerie, K.; Biemond, E.; Alfonso, G. C.; de Jeu, W. H. Crystallization under shear in isotactic polypropylene containing nucleators. *Polymer* **2008**, *49*, 3076−3083.

(17) Luo, F.; Geng, C.; Wang, K.; Deng, H.; Chen, F.; Fu, Q.; Na, B. New Understanding in Tuning Toughness of β-Polypropylene: The Role of β-Nucleated Crystalline Morphology. *Macromolecules* **2009**, *42*, 9325−9331.

(18) Chen, H. B.; Karger-Kocsis, J.; Wu, J. S.; Varga, J. Fracture toughness of α- and β-phase polypropylene homopolymers and random- and block-copolymers. *Polymer* **2002**, *43*, 6505−6514.

(19) Jacoby, P.; Bersted, B. H.; Kissel, W. J.; Smith, C. E. Studies on the β-crystalline form of isotactic polypropylene. *J. Polym. Sci., Part B: Polym. Phys.* **1986**, *24*, 461−491.

(20) Luo, F.; Wang, K.; Ning, N.; Geng, C.; Deng, H.; Chen, F.; Fu, Q.; Qian, Y.; Zheng, D. Dependence of mechanical properties on β-form content and crystalline morphology for β-nucleated isotactic polypropylene. *Polym. Adv. Technol.* **2011**, *22*, 2044−2054.

(21) Mollova, A.; Androsch, R.; Mileva, D.; Gahleitner, M.; Funari, S. S. Crystallization of isotactic polypropylene containing beta-phase nucleating agent at rapid cooling. *Eur. Polym. J.* **2013**, *49*, 1057−1065.

(22) Marco, C.; Gómez, M. A.; Ellis, G.; Arribas, J. M. Activity of a β-nucleating agent for isotactic polypropylene and its influence on polymorphic transitions. *J. Appl. Polym. Sci.* **2002**, *86*, 531−539.

(23) Bohaty, P.; Vlach, B.; Seidler, S.; Koch, T.; Nezbedova, E. ESSENTIAL WORK OF FRACTURE AND THE PHASE TRANSFORMATION IN β-iPP. *J. Macromol. Sci., Part B: Phys.* **2007**, *41*, 657−669.

(24) Varga, J.; Menyhárd, A. Effect of Solubility and Nucleating Duality of N,N'-Dicyclohexyl-2,6-naphthalenedicarboxamide on the Supermolecular Structure of Isotactic Polypropylene. *Macromolecules* **2007**, *40*, 2422−2431.

(25) Zhang, X.; Luster, B.; Church, A.; Muratore, C.; Voevodin, A. A.; Kohli, P.; Aouadi, S.; Talapatra, S. Carbon Nanotube−MoS2 Composites as Solid Lubricants. *ACS Appl. Mater. Interfaces* **2009**, *1*, 735−739.

(26) Benavente, E.; Santa Ana, M. A.; Mendizábal, F.; González, G. Intercalation chemistry of molybdenum disulfide. *Coord. Chem. Rev.* **2002**, *224*, 87−109.

(27) Luo, J.; Zhu, M. H.; Wang, Y. D.; Zheng, J. F.; Mo, J. L. Study on rotational fretting wear of bonded MoS2 solid lubricant coating prepared on medium carbon steel. *Tribol. Int.* **2011**, *44*, 1565−1570.

(28) Zhou, K.; Liu, J.; Wen, P.; Hu, Y.; Gui, Z. A noncovalent functionalization approach to improve the dispersibility and properties of polymer/MoS2 composites. *Appl. Surf. Sci.* **2014**, *316*, 237−244.

(29) Ma, L.; Chen, W.-X.; Li, H.; Xu, Z.-D. Synthesis and characterization of MoS2 nanostructures with different morphologies via an ionic liquid-assisted hydrothermal route. *Mater. Chem. Phys.* **2009**, *116*, 400−405.

(30) Frey, G. L.; Tenne, R.; Matthews, M. J.; Dresselhaus, M. S.; Dresselhaus, G. Raman and resonance Raman investigation of MoS2 nanoparticles. *Phys. Rev. B* **1999**, *60*, 2883−2892.

(31) Feng, X.; Tang, Q.; Zhou, J.; Fang, J.; Ding, P.; Sun, L.; Shi, L. Novel mixed−solvothermal synthesis of MoS2 nanosheets with controllable morphologies. *Cryst. Res. Technol.* **2013**, *48*, 363−368.

(32) Longo, C.; Savaris, M.; Zeni, M.; Brandalise, R. N.; Grisa, A. M. C. Degradation study of polypropylene (PP) and bioriented polypropylene (BOPP) in the environment. *Mater. Res.* **2011**, *14*, 442−448.

(33) Zhang, F.; Tang, Y.; Yang, Y.; Zhang, X.; Lee, C.-S. In-situ assembly of three-dimensional MoS2 nanoleaves/carbon nanofiber composites derived from bacterial cellulose as flexible and binder-free anodes for enhanced lithium-ion batteries. *Electrochim. Acta* **2016**, *211*, 404−410.

(34) Aurrekoetxea, J.; Sarrionandia, M. A.; Urrutibeascoa, I.; Maspoch, M. L. Effects of injection moulding induced morphology on the fracture behaviour of virgin and recycled polypropylene. *Polymer* **2003**, *44*, 6959−6964.

(35) Favaro, M. M.; Branciforti, M. C.; Bretas, R. E. S. A X-ray study of β-phase and molecular orientation in nucleated and non-nucleated injection molded polypropylene resins. *Mater. Res.* **2009**, *12*, 455−464.

(36) Hu, K. H.; Hu, X. G.; Wang, J.; Xu, Y. F.; Han, C. L. Tribological Properties of MoS2 with Different Morphologies in High-Density Polyethylene. *Tribol. Lett.* **2012**, *47*, 79−90.

(37) Wang, J.; Hu, K. H.; Xu, Y. F.; Hu, X. G. Structural, thermal, and tribological properties of intercalated polyoxymethylene/molybdenum disulfide nanocomposites. *J. Appl. Polym. Sci.* **2008**, *110*, 91−96.

(38) Dunckle, C. G.; Aggleton, M.; Glassman, J.; Taborek, P. Friction of molybdenum disulfide−titanium films under cryogenic vacuum conditions. *Tribol. Int.* **2011**, *44*, 1819−1826.

(39) Kalin, M.; Kogovšek, J.; Remškar, M. Mechanisms and improvements in the friction and wear behavior using MoS2 nanotubes as potential oil additives. *Wear* **2012**, *280-281*, 36−45.

(40) Sehaqui, H.; Kochumalayil, J.; Liu, A.; Zimmermann, T.; Berglund, L. A. Multifunctional Nanoclay Hybrids of High Toughness, Thermal, and Barrier Performances. *ACS Appl. Mater. Interfaces* **2013**, *5*, 7613−7620.

(41) De, B.; Voit, B.; Karak, N. Transparent Luminescent Hyperbranched Epoxy/Carbon Oxide Dot Nanocomposites with Outstanding Toughness and Ductility. *ACS Appl. Mater. Interfaces* **2013**, *5*, 10027−10034.

(42) Brostow, W.; Hagg Lobland, H. E.; Khoja, S. Brittleness and toughness of polymers and other materials. *Mater. Lett.* **2015**, *159*, 478−480.

(43) Hu, K. H.; Hu, X. G.; Xu, Y. F.; Sun, J. D. Synthesis of nano-MoS2/TiO2 composite and its catalytic degradation effect on methyl orange. *J. Mater. Sci.* **2010**, *45*, 2640−2648.